Indonesian Journal of Science & Technology

Journal homepage: http://ejournal.upi.edu/index.php/ijost/

# Multi-Distributed Activation Energy Model for Pyrolysis of Sugarcane Bagasse: Modelling Strategy and Thermodynamic Characterization

*Siti Jamilatun[1], Muhammad Aziz[2], Joko Pitoyo[1*]*

[1]Department of Chemical Engineering, Faculty of Industrial Technology, Universitas Ahmad Dahlan, Indonesia
[2]Institute of Industrial Science, The University of Tokyo 4-6-1 Komaba, Meguro-ku, Tokyo 153-8505, Japan
*Correspondence: E-mail: joko2107054001@webmail.uad.ac.id

## ABSTRACT

The multi-distributed activation energy model (multi-DAEM) is the most effective approach for outlining the kinetics model of biomass pyrolysis. The purpose of this study is to identify the optimal number and shape of the DAEM for sugarcane bagasse pyrolysis and to discuss its thermodynamic characteristics using the combination of multi-DAEM and differential thermal analysis (DTA). The heating rate of 10, 30, and 50 °C/min was employed. The results revealed that the multi-DAEM with five pseudo components and Weibull distribution shape gave the lowest relative root mean of the squared error (RRMSE) of 0.66% and 0.41%, respectively. Kinetic and thermodynamic studies showed that the 1st and 4th pseudo components which represent lignin, have activation energy ($E_0$) of 189.6 and 180.6 kJ/mol, and less endothermic or possibly exothermic properties. Meanwhile, the 2nd, 3rd, and 5th pseudo components which represent cellulose, hemicellulose, and moisture have activation energy ($E_0$) of 176.1, 152.2, and 145.6 kJ/mol, respectively, and endothermic properties.



## ARTICLE INFO

***Article History:***
*Submitted/Received 24 Dec 2022*
*First Revised 12 May 2023*
*Accepted 05 Jul 2023*
*First Available online 06 Jul 2023*
*Publication Date 01 Dec 2023*

***Keyword:***
*Bagasse pyrolysis,*
*Kinetic,*
*Multi-DAEM,*
*TG-DTA,*
*Thermodynamic.*

## 1. INTRODUCTION

One of Indonesia's major sources of farming waste is bagasse. (Pradana *et al*., 2019). Bagasse can be used as fuel in boilers and power generators (Ordonez-Loza *et al*., 2021). It is a lignocellulosic biomass that Several processes (including pyrolysis) can convert into fuel. (Jamilatun *et al*., 2022; Pradana *et al*., 2019). Pyrolysis is a thermal decomposition without an oxidizing agent (air or oxygen) (Guedes *et al*., 2018; Pitoyo *et al*., 2022). It is considered a superior method to other thermochemical conversions because of its versatility in choosing raw materials, wider temperature operational (300-600 °C), possible operation at atmospheric pressure, and its ability to produce three valuable products (solid, liquid, and gas) simultaneously (Jamilatun *et al*., 2019; Terry *et al*., 2021). Several research studies have been carried out related to the mechanism, operating parameters, and kinetics model of pyrolysis (Hameed *et al*., 2019; Kaczor *et al*., 2020; Wang *et al*., 2017).

There are two fundamental mathematical procedures to experimentally determine the kinetics of biomass pyrolysis's parameters: model-free and model-fitting methods (Cai *et al*., 2014). The former method, also called the iso-conventional method, assumes that the conversion value affects kinetic parameters like the frequency factor and activation energy (Aboyade *et al*., 2011). This method includes Miura differential method, Miura-Maki integral method, Coats-Redfern, Flynn-Wall-Ozawa, Kissinger, and Kissinger-Akahira-Sunose. This method is easier because it only requires linear regression (Bonilla *et al*., 2019; Sukarni, 2020; Zhao *et al*., 2020).

However, it has several areas for improvement, such as requiring a minimum of three experiments with different heating rates and not being suitable for multiple reactions (Vyazovkin *et al*., 2011). Sometimes it is difficult to find conversion derivatives to the activation energy due to significant variations in conversion to the activation energy (Cai *et al*., 2014).

The model-fitting method can be grouped into single-reaction and multi-reaction models. Multi-reaction models include the lumped kinetic model and DAEM. The lumped kinetic model assumes several parallel reactions, each with their individual activation energy. At the same time, DAEM assumes that the decomposition mechanism involves multiple independent parallel reactions with various activation energies for each reaction (see https://www.american.edu/sis/centers/carbon/removal; Sonobe & Worasuwannarak, 2008; Vyazovkin *et al*., 2011).

DAEM explains the kinetics of biomass pyrolysis, the mechanism of thermally degradable materials, and complex chemical systems such as coal pyrolysis (Quan *et al*., 2009). However, the model-fitting method is weak, as the obtained kinetic parameters provide accurate data fitting at only one heating rate (Várhegyi *et al*., 2011).

The distributional shape of DAEM describes different behavior and kinetic mechanisms. The exact shape of the distribution of activation energy is unknown. Its shape can be grouped into two types, symmetrical and asymmetrical. Symmetric distribution shapes include Gaussian, Gumbel, Cauchy, and Logistic, with the Gaussian distribution being the most widely applied (Dhaundiyal & Singh, 2016; Tran *et al*., 2016). However, the Gaussian distribution has a weakness as it is symmetrical, while the actual distribution is asymmetrical (Burnham & Braun, 1998). This makes asymmetric distributions such as the Weibull and Gamma distributions more attractive to be implemented (Cai & Liu, 2007; Kuo-Chao *et al*., 2009). In addition to the shape of the distribution, the number of distributions or pseudo-components is an important factor. It determines the accuracy of a simulation and the complexity of calculations. Too few distributions reduce

DOI: https://doi.org/10.17509/ijost.v8i3.60175
p- ISSN 2528-1410 e- ISSN 2527-8045

the accuracy of a model, while too many require high computational costs. Three distribution numbers have been broadly employed to describe the pyrolysis of biomass (Cai *et al*., 2014). The use of a distribution number of four or five has also been employed to describe the thermal decomposition of plastic waste, marine biomass, and also lignocellulosic biomass (Burra & Gupta, 2018; Kristanto *et al*., 2021; Y. Lin *et al*., 2019). Choosing the correct number and shape of the model can simplify the complexity of the calculations while increasing the prediction ability and accuracy of the simulations performed.

Thermogravimetric differential thermal analysis (TG-DTA) is an analysis method generally used to study the thermal decomposition of biomass (Viju *et al*., 2018). TG-DTA can simultaneously calculate weight change and differential heat flow as a function of time and temperature. DTA measurement is based on the difference between the reference and sample temperatures. The thermodynamic properties of the pseudo component have a significant correlation with the reaction enthalpy profile (Kristanto *et al*., 2021). To our best knowledge, systematic determination of the number and shape of DAEM is rarely investigated, while the use of the relationship between multi-DAEM and DTA profile to explain the thermodynamic properties of the involved pseudo components has never been performed.

This paper aims to determine the number and shape of the best DAEM that can accurately describe the decomposition process in bagasse pyrolysis and, at the same time, discuss the thermodynamic properties of each pseudo component based on the relationship between multi-DAEM and DTA profile.

## 2. METHODS

### 2.1. Materials

Bagasse was obtained from PT Madukismo Yogyakarta. Samples were washed to remove the impurities, then oven dried for 24 h. After drying, the sample was crushed and sieved to get a grain size of 60 mesh. **Table 1** lists the results of the proximate, ultimate, and compositional analyses.

### 2.2. Thermogravimetric Pyrolysis

Pyrolysis was carried out using a simultaneous TG-DTA Hitachi STA-200RV at atmospheric pressure in an inert nitrogen atmosphere. The sample is weighed as much as 6-10 mg and placed in a platinum pan, a small sample weight (6-10 mg) is taken to reduce mass and heat transfer barriers ( Y.-C. Lin *et al*., 2009; Várhegyi *et al*., 2011). Constant heating rates of 10, 30, and 50 °C/min were utilized to heat the sample from 30 to 900°C. $N_2$ gas with high purity (99.99%) is flown at 100 mL/min to obtain an inert condition. In TG-DTA, there is a thermal lag at high heating rates between the thermocouple reading and the sample's actual temperature. Therefore 10 °C/min heating rate was selected to evaluate the thermodynamic properties based on the DTA profile to minimize the occurrence of thermal lag (Jr & Grønli, 2003).

**Table 1**. Proximate and elemental analysis of bagasse.

| Ultimate analysis | Value (wt.%) | Proximate analysis | Value (wt.%) | Composition analysis | Value (wt.%) |
|---|---|---|---|---|---|
| C | 42.50 | Moisture | 3.83 | Cellulose | 45.82 |
| H | 6.17 | Volatile matter | 21.95 | Hemicellulose | 20.20 |
| O | 51.0 0 | Fixed carbon | 71.60 | Lignin | 21.32 |
| N | 0.23 | Ash | 2.60 | | |
| S | 0.10 | | | | |

DOI: https://doi.org/10.17509/ijost.v8i3.60175
p- ISSN 2528-1410 e- ISSN 2527-8045

### 2.3. Kinetic Modeling

Kinetic modeling is important to determine the optimal kinetic parameters, pre-exponential factor (*A*), and activation energy (*E*). In this study, the n$^{th}$-order reaction model and DAEM were used. The n$^{th}$-order reaction model is shown by Equation [1].

$$\alpha(\mathrm{T}) = 1 - \left[1 - (1-n)\int_{\mathrm{T0}}^{\mathrm{T}} \frac{A}{\beta}\exp\left(-\frac{E}{RT}\right)dT\right]^{\frac{1}{(1-n)}} \quad (1)$$

where $\beta$ is the heating rate, $T$ is the temperature at time t, $T_0$ is the initial temperature, $R$ is the universal gas constant, and $n$ is the reaction order. Moreover, the degree of conversion is formulated by Equation [2].

$$\alpha(\mathrm{T}) = \frac{m_i - m_T}{m_i - m_f} \quad (2)$$

where $m_i$ is the initial mass of the sample, $m_T$ is the mass of the sample at temperature $T$, and $m_f$ is the final mass of the sample. The equation for single-DAEM is shown in Equation [3].

$$\alpha(\mathrm{T}) = 1 - \int_0^{\infty} \exp\left[-\int_{\mathrm{T0}}^{\mathrm{T}} \frac{A}{\beta}\exp\left(-\frac{E}{RT}\right)dT\right] f(E)dE \quad (3)$$

Biomass is a complex chemical material consisting of multiple pseudo components that do not interact with each other during the thermal decomposition process; hence, multi-DAEM is needed to accurately describe the decomposition process (Vyazovkin *et al.*, 2011). To explain the contribution of each pseudo component, weighting; or contribution factor; $c_j$ was introduced (Kristanto *et al.*, 2021), and the equation for multi-DAEM is shown in Equation [4].

$$\alpha(\mathrm{T}) = 1 - \sum_{j=1}^{Nd} cj \int_0^{\infty} \exp\left[-\int_{\mathrm{T0}}^{\mathrm{T}} \frac{A_j}{\beta}\exp\left(-\frac{E}{RT}\right)dT\right] f_j(E)dE \quad (4)$$

Here *Nd* is the number of distributions, and $f_j(E)$ is the distribution function or the shape of DAEM. In this study, seven shapes of DAEM were used: Gaussian, Logistic, Gumbel, Cauchy, Weibull, Gamma, and Rayleigh. **Table 2** shows the distribution function of each DAEM. There is no exact analytical solution to the problem since it has double integrals, inner integrals *dT*, and outer integrals *dE*. (Mcguinness *et al.*, 1999; Órfão, 2007; Tran *et al.*, 2016). In this study, the temperature integral estimation suggested by Cai *et al.* (2006) was applied to solve the inner integral *dT* and the trapezoidal integration rule to solve the outer integral *dE*. The pre-exponential factor ($A_j$) was determined by setting the initial optimization value close to the values in the literature, namely $10^{14.13}$, $10^{13.71}$, $10^{13.90,}$ and $1.67\text{x}10^{13}$/s for hemicellulose, cellulose, lignin, and unknown components, respectively (Várhegyi *et al.*, 2011). The upper limit of outer integral *dE* is 500 kJ/mol (Güneş & Güneş, 1999).

**Table 2**. Type of distribution function used in this research.

| Distributions | Distribution Function, $f$(E) | Mean value of $E$ | Standard deviation of $E$ |
|---|---|---|---|
| Gaussian | $f(\mathrm{E}) = \frac{1}{\sigma\sqrt{2\pi}}\exp\left[-\frac{(E-E_0)^2}{2\sigma^2}\right]$ | $E_0$ | $\sigma$ |
| Logistic | $f(E) = \frac{1}{4\sigma}\mathrm{sech}\frac{(E-E_0)}{2\sigma}$ | $E_0$ | $\sigma$ |
| Gumbel | $f(E) = \frac{1}{\sigma}\exp\left[-\left(\frac{E-E_0}{\sigma} + \exp\left\{-\left(\frac{E-E_0}{\sigma}\right)\right\}\right)\right]$ | $E_0$ | $\sigma$ |
| Cauchy | $f(\mathrm{E}) = \frac{1}{\pi\sigma}\left[1 + \left(\frac{E-E_0}{\sigma}\right)^2\right]^{-1}$ | $E_0$ | $\sigma$ |
| Weibull | $f(E) = \frac{k}{\lambda}\left(\frac{E}{\lambda}\right)^{k-1}\exp\left[-\left(\frac{E}{\lambda}\right)^k\right]$ | $\lambda\Gamma\left(1+\frac{1}{k}\right)$ | $\lambda^2\left[\Gamma\left(1+\frac{2}{k}\right) - \left\{\Gamma\left(1+\frac{1}{k}\right)\right\}^2\right]$ |
| Gamma | $f(\mathrm{E}) = \frac{E^{k-1}}{\Gamma(k)\theta^k}\exp\left(-\frac{E}{\theta}\right)$ | $k\theta$ | $k\theta^2$ |
| Rayleigh | $f(E) = \frac{E}{\sigma^2}\exp\left(-\frac{E^2}{2\sigma^2}\right)$ | $\sigma\sqrt{\frac{\pi}{2}}$ | $\left(\frac{4-\pi}{2}\right)\sigma^2$ |

DOI: https://doi.org/10.17509/ijost.v8i3.60175
p- ISSN 2528-1410 e- ISSN 2527-8045

The objective function in Equation (5) was minimized to achieve the kinetic parameters. The objective function was determined by summing the square errors between the experimental and the DAEM simulation data. The objective function was minimized using the Matlab software package, i.e., the *fmincon* function using the sequential quadratic programming (SQP) algorithm. This optimization used a maximum iteration of 1000 and a maximum function evaluation of 5000 for all distributed activation energy models (DAEM). The range of values used in the literature is the basis for the optimization's constraints (Várhegyi *et al*., 2011). The value of the $E_0$ was taken from 100 to 350 kJ/mol, the standard deviation ($\sigma$) was taken from 0 to 70 kJ/mol, the pre-exponential factor ($Aj$) was selected from $10^{10}$ to $10^{20}$/s, and the contribution factor ($c_j$) was selected from 0 to 1.

$$\mathrm{SSE} = \sum_{i=1}^{np}\left[\alpha_{exp,i}(\mathrm{T}) - \alpha_{model,i}(\mathrm{T})\right]^2 \quad (5)$$

$\alpha_{exp,i}$ and $\alpha_{model,i}$ are the degree of conversion of the experimental data and the model, respectively, and *np* is the number of data points. The quality of fitting was evaluated using the relative root mean of the square error (RRMSE) and the coefficient of determination ($R^2$), as shown in Equations [6] and [7] (Feng *et al*., 2022).

$$\mathrm{RRMSE} = \frac{\sqrt{\frac{1}{np}\sum_{i=1}^{np}\left[\alpha_{exp,i}(\mathrm{T}) - \alpha_{model,i}(\mathrm{T})\right]^2}}{\bar{\alpha}_{exp,i}} \times 100\% \quad (6)$$

$$\mathrm{R}^2 = 1 - \frac{\sum_{i=1}^{np}\left[\alpha_{exp,i}(\mathrm{T}) - \alpha_{model,i}(\mathrm{T})\right]^2}{\sum_{i=1}^{np}\left[\alpha_{exp,i}(\mathrm{T}) - \bar{\alpha}_{exp,i}(\mathrm{T})\right]^2} \quad (7)$$

where $\bar{\alpha}_{exp,i}(\mathrm{T})$ is the average value of the experimental data. **Figure 1** shows the optimization algorithm to determine the optimal kinetic parameters.

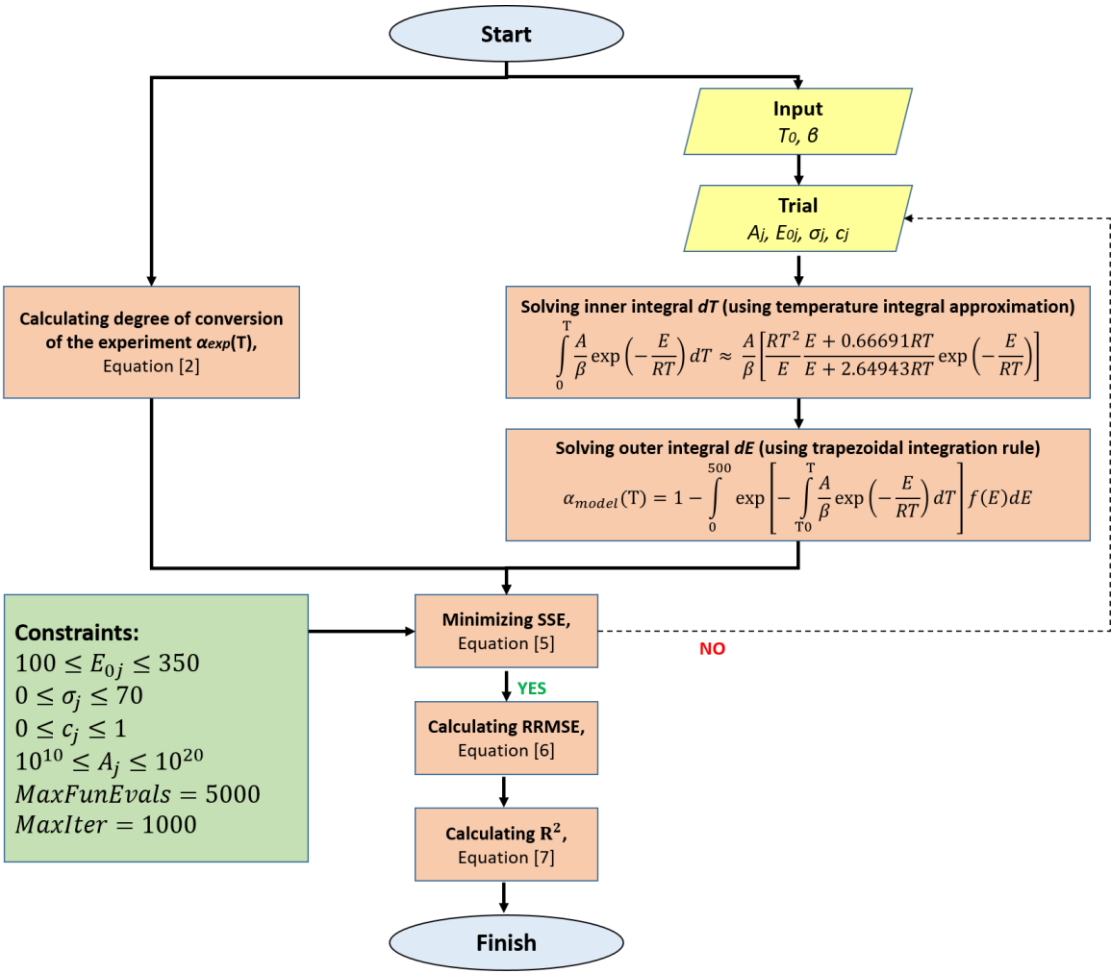


**Figure 1**. Kinetic parameters calculation algorithm.

DOI: https://doi.org/10.17509/ijost.v8i3.60175
p- ISSN 2528-1410 e- ISSN 2527-8045

## 3. RESULTS AND DISCUSSION

### 3.1. TG-DTA of Bagasse

**Figure 2** presents the results of the TG-DTA analysis of bagasse at a heating rate of 10, 30, and 50 °C/min. The heating rate dramatically affects the decomposition characteristics. Considering the TGA's characteristics, the high heating rate reduced the time needed for decomposition from 48.27 min at a heating rate of 10 °C/min to 17.98 and 12.09 min at 30 and 50 °C/min, respectively. On the other hand, a high heating rate reduced the total solids conversion from 97.14% at a heating rate of 10 °C/min to 89.83 and 91.48% at a heating rate of 30 and 50 °C/min, respectively. This is likely because the high heating rate triggers a secondary decomposition reaction that converts volatile materials into char (Guedes *et al.*, 2018). Based on the characteristics of DTG (**Figure 2a**), the peak temperature was moved to the right by increasing the heating rate from 332.58°C at a heating rate of 10°C/min to 350.87 and 360.17°C at heating rates of 30 and 50 °C/min, respectively. Based on the characteristics of the DTA, the high heating rate causes the loss of the peak appearance on the DTA curve. This is probably brought on by the thermal delay between the sample temperature and thermocouple measuring (Jr & Grønli, 2003). This suggests the use of low heating rates in studying biomass decomposition kinetics to avoid the loss of peaks on the DTA or DTG curves. The DTG curve shows a peak at 332.58 °C, a shoulder at 300 °C, and tailings at a temperature range of 365-550 °C. The peak is associated with cellulose decomposition, the shoulder is associated with hemicellulose decomposition, and the tailings at the end of the pyrolysis temperature are associated with lignin decomposition.

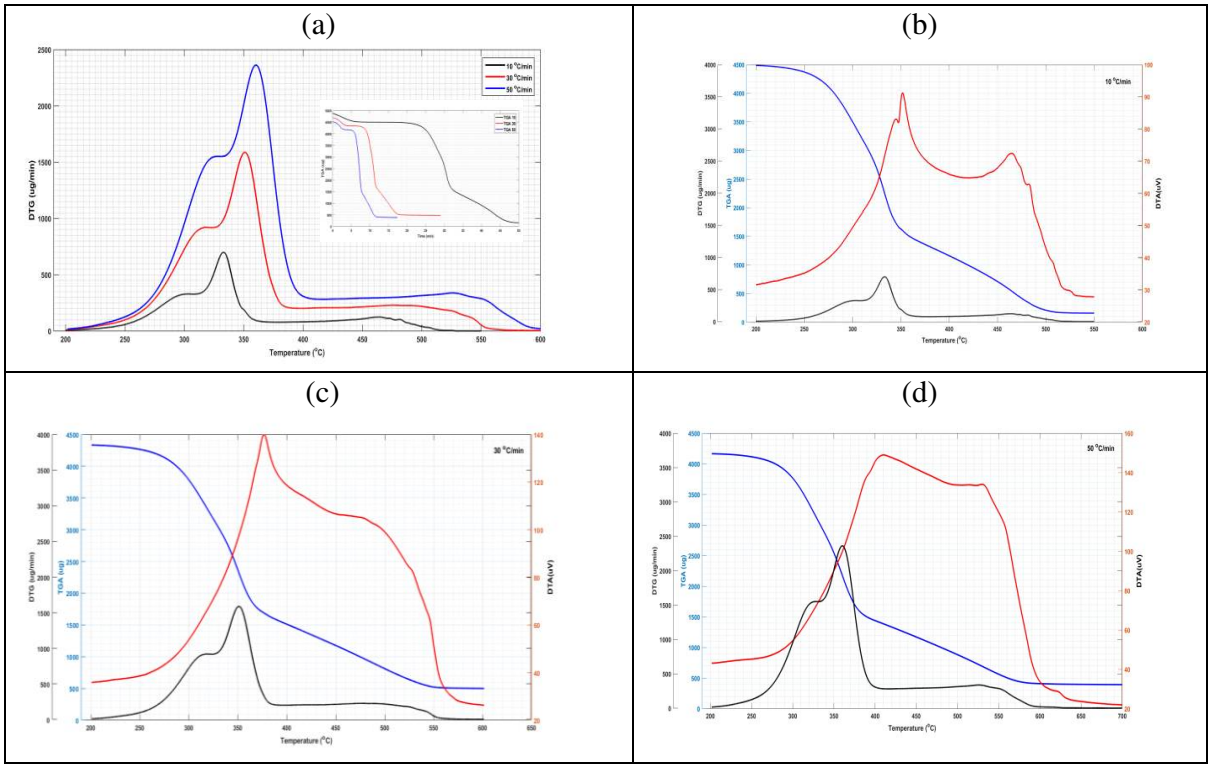


**Figure 2**. The curve of several parameters: (a) DTG at different temperatures, (b) TG-DTA at a heating rate of 10 °C/min, (c) TG-DTA at a heating rate of 20 °C/min, and (d) TG-DTA at a heating rate of 30 °C/min.

DOI: https://doi.org/10.17509/ijost.v8i3.60175
p- ISSN 2528-1410 e- ISSN 2527-8045

### 3.2. Determination Number of Distribution

**Figure 3** depicts how the number of distributions has an impact on fitting quality using five distribution numbers Gaussian. One Gaussian shows the most significant deviation among the five distribution numbers, and this is because of the limitations of one Gaussian in describing the multiple reactions that occur in biomass decomposition. **Figure 3a** shows that two, three, four, and five Gaussian provide overlapping data fittings. From **Figure 3b**, it can be seen clearly that the five Gaussians show the lowest RRMSE.

**Table 3** shows that using five Gaussian gives one distribution (the 3rd pseudo component) with a reasonably low contribution factor. Using a distribution number of more than five will result in several pseudo components with a relatively low contribution factor, which has no significant role in the reaction, and instead results in high computational complexity. Thus, it is not optimal. From the figure, moreover, it can be seen that the number of peaks on the DTG curve can indicate the number of distributions which can be used in the DAEM (Kristanto *et al*., 2021).

### 3.3. Determination Shape of The Distribution

The evaluation was performed on various shapes of DAEM such as Gaussian, Logistic, Gumbel, Cauchy, Weibull, Gamma, Rayleigh, and Reaction orders (non-DAEM) to obtain optimal conditions (providing a total RRMSE is minimum).

**Figure 4** shows that the Gamma, Rayleigh, and Reaction order models provide a high value of total RRMSE. Meanwhile, the Gaussian, Logistic, Gumbel, Cauchy, and Weibull models provide accurate results, as shown by the overlap of the graphs in **Figure 4a** and the low total RRMSE in **Figure 4b**.

**Table 3** shows a good fitting quality of the five models with a coefficient of determination ≥ 0.9998. Weibull best fits the five models (Kuo-Chao *et al*., 2009), characterized by the lowest RRMSE value. The reason is that the actual energy distribution in the biomass' thermal decomposition is asymmetrical, especially during the initial and final stages. Weibull model is an asymmetrical distribution model, so it can provide good fitting, especially at the beginning and end of the thermal decomposition (Cai & Liu, 2007; Kuo-Chao *et al*., 2009), as shown in **Figure 6**.

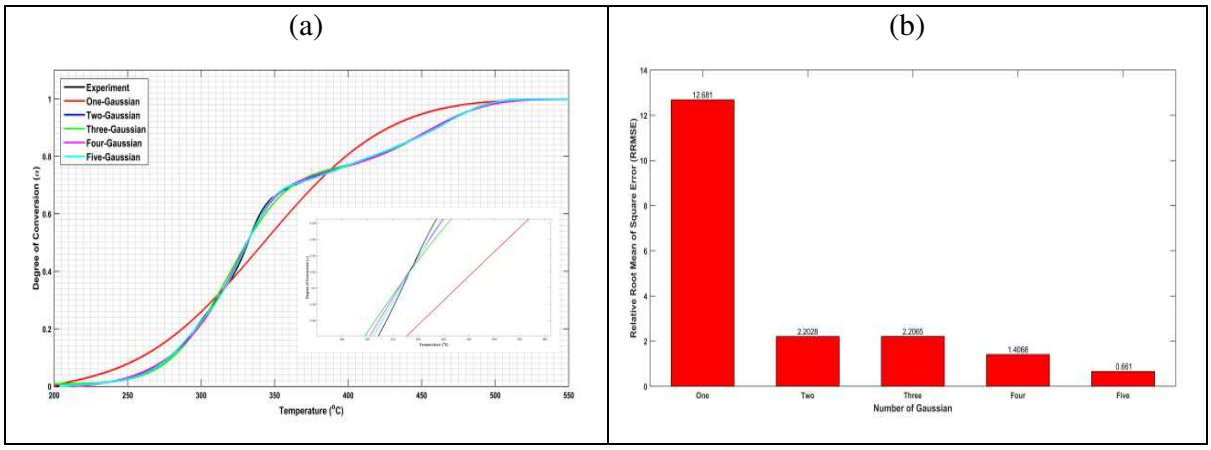


**Figure 3**. Identification of different numbers of Gaussian DAEM: (a) fitting data model and (b) calculated RRMSE.

DOI: https://doi.org/10.17509/ijost.v8i3.60175
p- ISSN 2528-1410 e- ISSN 2527-8045

**Table 3**. Kinetic and statistic parameters for bagasse pyrolysis.

| Shape of DAEM | Kinetics parameter | Pseudo component | | | | |
|---|---|---|---|---|---|---|
| | | 1st | 2nd | 3rd | 4th | 5th |
| Weibull | $c$ | 0.2029 | 0.4791 | 0.0101 | 0.1375 | 0.1705 |
| | $E_0$ | 189.6090 | 176.0650 | 145.6006 | 180.6271 | 152.2513 |
| | $\sigma$ | 16.7104 | 0.8478 | 6.0524 | 60.3042 | 1.1902 |
| | RRMSE (%) | | | 0.6162 | | |
| | $R^2$ | | | 1.0000 | | |
| Gaussian | $c$ | 0.1870 | 0.5143 | 0.0465 | 0.1344 | 0.1534 |
| | $E_0$ | 190.3440 | 164.6107 | 150.0123 | 195.8034 | 162.4114 |
| | $\sigma$ | 3.0611 | 0.3026 | 22.0800 | 7.6443 | 0.2139 |
| | RRMSE (%) | | | 0.6610 | | |
| | $R^2$ | | | 0.9999 | | |
| Logistic | $c$ | 0.1758 | 0.4990 | 0.0660 | 0.1098 | 0.1524 |
| | $E_0$ | 190.1544 | 164.7257 | 184.1894 | 184.3085 | 162.4515 |
| | $\sigma$ | 1.1206 | 0.1005 | 16.7588 | 3.2011 | 0.7639 |
| | RRMSE (%) | | | 0.7384 | | |
| | $R^2$ | | | 0.9999 | | |
| Gumbel | $c$ | 0.1688 | 0.3754 | 0.0322 | 0.2439 | 0.1753 |
| | $E_0$ | 189.2224 | 164.0643 | 196.3672 | 169.5746 | 161.4599 |
| | $\sigma$ | 0.2932 | 0.5308 | 16.4970 | 10.5493 | 4.4010 |
| | RRMSE (%) | | | 1.2104 | | |
| | $R^2$ | | | 0.9998 | | |
| Cauchy | $c$ | 0.1821 | 0.4434 | 0.0000 | 0.1805 | 0.1510 |
| | $E_0$ | 188.8274 | 164.2228 | 199.0293 | 180.0004 | 162.3227 |
| | $\sigma$ | 0.2869 | 0.2958 | 17.4544 | 6.0263 | 0.0653 |
| | RRMSE (%) | | | 1.1249 | | |
| | $R^2$ | | | 0.9998 | | |

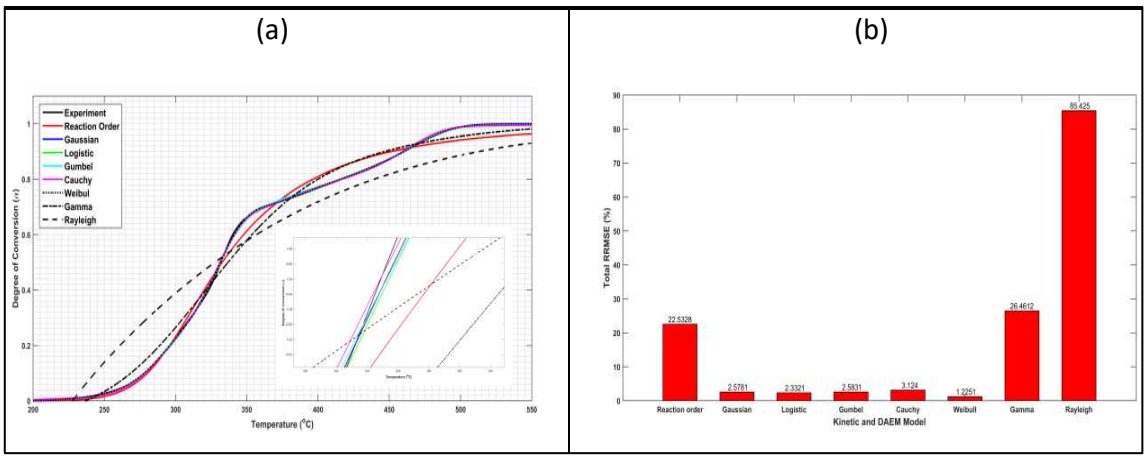


**Figure 4**. Identification of different shapes of multi-DAEM: (a) fitting data model and (b) calculated RRMSE.

### 3.4. Sensitivity Analysis of DAEM Kinetic Parameter

**Figure 5** reveals the local sensitivity analysis of the parameters obtained from DAEM. Local sensitivity analysis is evaluated on specific parameters (Sciacovelli & Verda, 2012). Sensitivity analysis is applied to assess the parameters' robustness in different input data. The x-axis shows deviations from optimal parameters, the y-axis shows the kinetic parameters of DAEM, and the different colors in contours show

DOI: https://doi.org/10.17509/ijost.v8i3.60175
p- ISSN 2528-1410 e- ISSN 2527-8045

the RRMSE values. At the same value of x, the closer to the yellow area the higher the RRMSE value and the more sensitive. It can be seen from **Figure 5** that the standard deviation ($\sigma$) is the most sensitive parameter among the existing parameters, marked by the number of contour areas with the yellow color. Meanwhile, the activation energy ($E_0$) and pre-exponential factor ($A$) have relatively excellent robustness. The $E_0$ and $A$ not sensitive when deviated from the optimal value indicated by the low value of RRMSE.

### 3.5. Kinetic Study of Bagasse Pyrolysis

**Figure 6** shows the DTG curve formed from the differentiation of experimental TGA data and the DAEM simulation using five pseudo components. Matching the number and shape of peaks between the DTG experiment and the DAEM simulation is needed to accurately describe the kinetics of the decomposition reaction (Kristanto *et al*., 2021). It can be seen from **Figure 6** that all DAEMs exhibit four major pseudo components (the 1st, 2nd, 4th, and 5th pseudo components) and one minor pseudo component (the 3rd pseudo component). Based on the Weibull model, at a temperature range of less than 250 °C, a minor pseudo component (3rd pseudo component) was decomposed with an $E_0$ of 145.60 kJ/mol and a contributing factor of 0.0101, which probably represents the decomposition of bound moisture and light volatiles.

In the range of 215-325°C, the 5th pseudo component decomposition occurred with an $E_0$ of 152.25 kJ/mol, a standard deviation of 1.19 kJ/mol, and a contributing factor of 0.17, which probably represents the hemicellulose decomposition. In the range of 245-370°C, the 2nd pseudo component decomposition occurred with an $E_0$ of 176.06 kJ/mol, a standard deviation of 0.85 kJ/mol, and a contributing factor of 0.48, which probably represents the cellulose decomposition.

In the range of 280-525 °C, the 1st and 4th pseudo component decomposition occurred with $E_0$ of 189.61 and 181.16 kJ/mol, standard deviations ($\sigma$) of 26.72 and 60.30 kJ/mol, and contributing factors of 0.2029 and 0.1375, respectively. This represents the decomposition of lignin and char. The appearance of several pseudo components in lignin decomposition was also reported in a previous study (Kristanto *et al*., 2021).

**Figure 7** shows the activation energy distribution of the five pseudo components during bagasse pyrolysis. The order of appearance of the peaks in the figure corresponds to the appearance of the pseudo components on the DTG curve. From the figure, the narrowest activation energy distribution range is seen in the 2nd pseudo component as reported by Huber *et al*., with an activation energy of 172-178 kJ/mol and a standard deviation of 0.85 kJ/mol. This range is included in cellulose's activation energy distribution range (Quan *et al*., 2016).

The distribution of the 5th pseudo component's activation energy is more comprehensive than that of the 2nd pseudo component, with an activation energy distribution of 146-155 kJ/mol and a standard deviation of 1.19 kJ/mol, belonging to the hemicellulose distribution range (J. Zhang *et al*., 2014).

At last, the 1st and 4th pseudo components have the widest distribution of the activation energy, in the range of 155-200 kJ/mol, and standard deviations of 16.71 and 60.30 kJ/mol . This indicates that the two components have a complex structure, and the decomposition arises over a broad temperature range, as in lignin decomposition (Jiang *et al*., 2010; Wang *et al*., 2015).

DOI: https://doi.org/10.17509/ijost.v8i3.60175
p- ISSN 2528-1410 e- ISSN 2527-8045

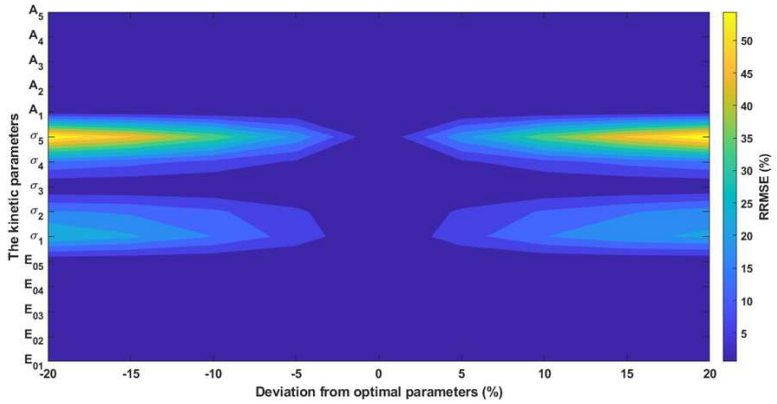


**Figure 5**. The local sensitivity analysis of multi-DAEM.

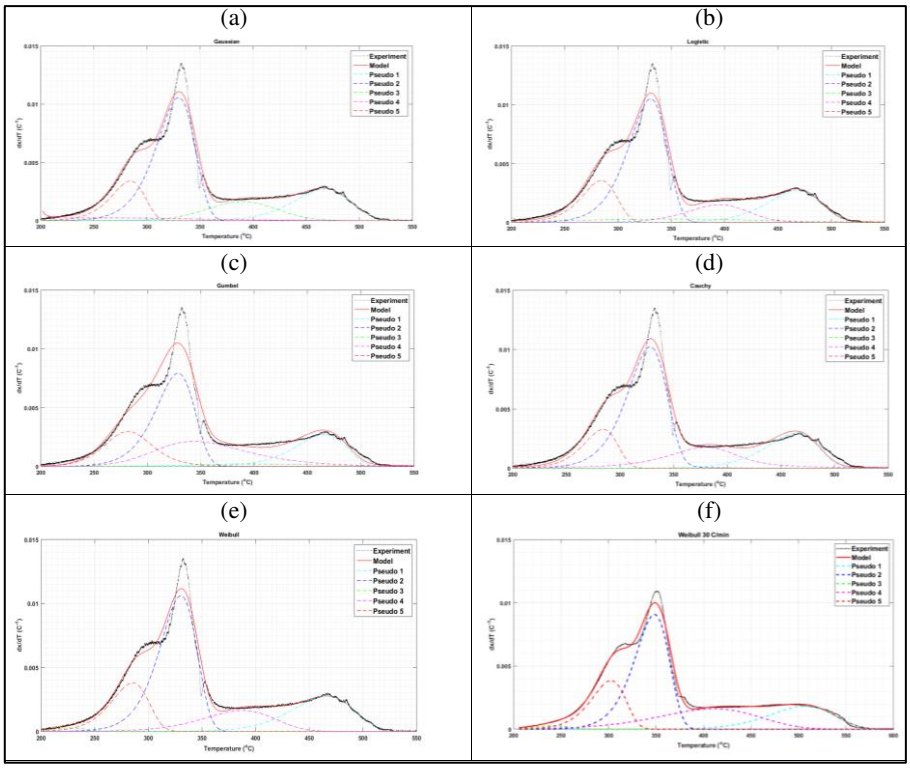


**Figure 6**. Experimental and simulation DTG of bagasse with multi-DAEM at heating rate of 10 °C/min using: (a) Gaussian, (b) Logistic, (c) Gumbel, (d) Cauchy, (e) Weibull, and (f) Weibull distribution at 30 °C/min.

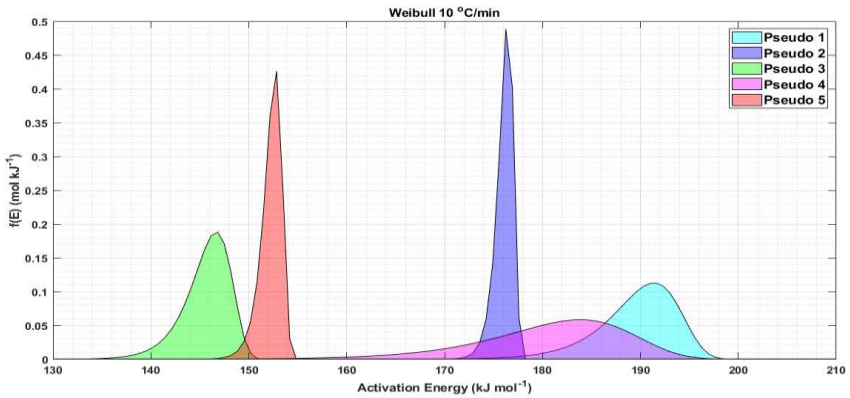


**Figure 7**. Activation energy distribution of multi-DAEM for pyrolysis of bagasse.

DOI: https://doi.org/10.17509/ijost.v8i3.60175
p- ISSN 2528-1410 e- ISSN 2527-8045

### 3.6. Thermodynamic characterization

The DTA instrument can determine heat flow in the reaction based on the temperature difference between the sample and reference for a fixed amount of heat input (Zhang *et al.*, 2008). The sample temperature remains constant for the endothermic reaction, so the heat flow (DTA) value is higher, whereas, in the exothermic reaction, the heat flow (DTA) value is lower. Using the relationship between DTA and the distribution of pseudo components in DTG, it is possible to understand the thermodynamic properties of each pseudo component and biomass decomposition behavior.

**Figure 8** shows the relationship between TGA, DTA, and multi-DAEM simulation, as also several stages for thermodynamic characterization. Each stage shows different temperature ranges, conversions, pseudo-component contributions, heat flow, and thermodynamic properties, as shown in **Table 4**. At the temperature of 200-250 °C or stage I of 3.7 µV, a slight increase in the DTG curve is accompanied by a slight increase in DTA value, representing the decomposition reaction of the 3rd pseudo component.

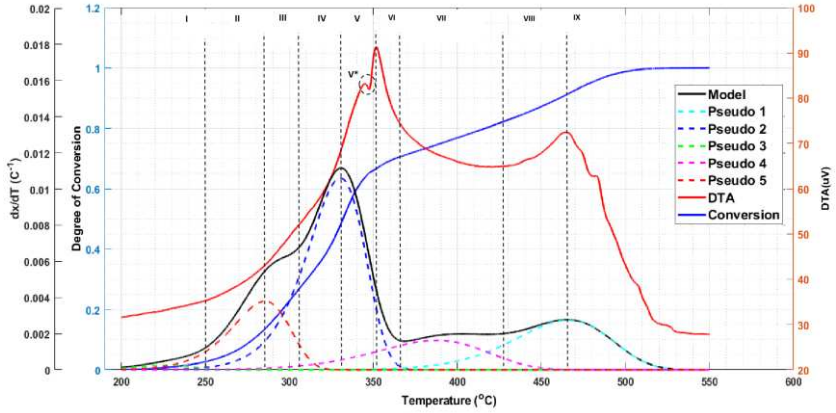


**Figure 8**. Comparison of TGA, DTA, and calculated DTG.

**Table 4**. Thermodynamic characterization of bagasse pyrolysis.

| Stage | Temperature (°C) | Conversion (%) | Pseudo component Contribution (%)** | Heat flow (µV ) | Thermodynamic properties |
|---|---|---|---|---|---|
| I | 200-250 | 2.59 | 2nd pseudo: 11.44<br>5th pseudo: 88.56 | 31-58-35.28 | endothermic |
| II | 250-285 | 13.33 | 2nd pseudo: 29.08<br>5th pseudo: 70.92 | 35.28-43.01 | endothermic |
| III | 285-305 | 26.28 | 2nd pseudo: 74.41<br>5th pseudo: 22.46<br>4th pseudo: 3.13 | 43.01-51.76 | endothermic |
| IV | 305-330 | 47.64 | 2nd pseudo: 95.11<br>4th pseudo: 4.89 | 51.76-68.31 | endothermic |
| V | 330-352 | 66.73 | 2nd pseudo: 76.63<br>4th pseudo: 23.37 | 68.31-91.31 | More endothermic |
| V* | 345-347.6 | 65.32 | 2nd pseudo: 90.93<br>4th pseudo: 9.07 | 83.11-81.92 | Less endothermic/ possibly exothermic |
| VI | 352-368 | 71.08 | 1st pseudo: 5.04<br>4th pseudo: 94.96 | 91.31-72.88 | Less endothermic/ possibly exothermic |
| VII | 368-430 | 82.80 | 1st pseudo: 73.02<br>4th pseudo: 26.98 | 72.88-65.05 | Exothermic |
| VIII | 430-465 | 91.10 | 1st pseudo: 100.00 | 65.05-72.47 | Endothermic |
| IX | 465-550 | 100.00 | 1st pseudo: 100.00 | 72.47-27.86 | Less endothermic/ possibly exothermic |

Note: **At the final temperature of each stage

DOI: https://doi.org/10.17509/ijost.v8i3.60175
p- ISSN 2528-1410 e- ISSN 2527-8045

This reaction may be related to the dehydration of active cellulose or bound moisture, which is endothermic. A sharp increase in DTA value of 56.03 µV occurred at a temperature range of 250-330 °C or stage II-IV, after the presence of the 2nd pseudo component. This indicates an endothermic reaction during the decomposition of the 2nd and 5th pseudo components representing cellulose and hemicellulose, respectively. The higher 2nd pseudo component contribution than the 5th reveals the more endothermicity of the 2nd pseudo component. The endothermicity of the 2nd pseudo component is related to the depolymerization of cellulose. There is a fluctuation in the DTA value between 352-550 °C or stages VI-IX. This indicates that the decomposition of the 1st and 4th pseudo components, which represent the decomposition of lignin, involves exothermic and endothermic reactions (Kristanto *et al*., 2021; Yang *et al*., 2007), with the exothermic tendency of the 4th pseudo component.

Thermodynamic parameters such as *A*, $E_0$, enthalpy ($\Delta H°$), entropy ($\Delta S°$), and Gibbs free energy ($\Delta G°$) are important for understanding the behavior of a chemical or physical process (Khajehzadeh *et al*., 2020). The thermodynamic parameter is obtained using the equation provided by Kim *et al*. (Kim *et al*., 2010) at the peak temperature of each pseudo component because that temperature gives the highest reaction rate (Aamer *et al*., 2017). A high *A* value improves both the reaction rate and the frequency of molecular collisions. The $E_0$ and $\Delta H°$ values indicate the minimum energy needed for a reaction and the low $E_0$ and $\Delta H°$ values increase the reaction rate. A high $\Delta S°$ indicates a high degree of disorder which has implications for increasing spontaneous reactions, high reactivity, and increasing reaction rates. Meanwhile, the high $\Delta G°$ decreases the spontaneous reaction. Thermodynamic parameters of the bagasse pyrolysis are summarized in **Table 5**.

Based on **Table 5**, the 3rd pseudo component has the lowest $E_0$, $\Delta H°$, and $\Delta G°$ values and the highest *A* and $\Delta S°$ values; hence, it has a high tendency for the reaction to occur spontaneously. The 5th pseudo component, which represents hemicellulose, has relatively low $E_0$, $\Delta H°$, and $\Delta G°$ values and relatively high *A* and $\Delta S°$ values. Therefore, it has a relatively high tendency for spontaneous reactions to occur but is still weaker than the 3rd pseudo component. The 2nd pseudo component, which represents cellulose, has relatively low $E_0$, $\Delta H°$, and $\Delta G°$ values, while *A* and $\Delta S°$ values are relatively high. Hence, it has a fairly high tendency for spontaneous reactions to occur but is still weaker than the 3rd and 5th pseudo components. Meanwhile, the 1st and 4th pseudo components, which represent lignin, have high $E_0$, $\Delta H°$, and $\Delta G°$ values but low *A* and $\Delta S°$ values, so spontaneous reactions have a low tendency to occur (Xu & Chen, 2013).

**Table 5**. Thermodynamic parameters for bagasse pyrolysis.

| Pseudo component | $E_0$ (kJ/mol) | *A* ($s^{-1}$) | $\Delta H°$ (kJ/mol) | $\Delta S°$ (kJ/mol) | $\Delta G°$ (kJ/mol) |
|---|---|---|---|---|---|
| 1st | 189.609 | 1.09594E+13 | 183.472 | -0.011 | 191.689 |
| 2nd | 176.065 | 1.03117E+15 | 171.050 | 0.028 | 153.964 |
| 3rd | 145.600 | 1.30756E+15 | 141.459 | 0.032 | 125.571 |
| 4th | 180.6271 | 1.08759E+14 | 175.155 | 0.009 | 169.296 |
| 5th | 152.251 | 1.04291E+14 | 147.611 | 0.01 | 142.072 |

DOI: https://doi.org/10.17509/ijost.v8i3.60175
p- ISSN 2528-1410 e- ISSN 2527-8045

## 4. CONCLUSION

TG-DTA pyrolysis of bagasse has been investigated using a DAEM to determine the optimal number and shape of DAEM. The combination of DAEM and DTA can be used to study the thermodynamic properties of bagasse pyrolysis. The results show that the multi-DAEM with five pseudo components gave the lowest RRMSE of 0.66%. Based on the shape of the multi-DAEM, the Weibull distribution gives the lowest average RRSME value of 0.41%. Based on the kinetic and thermodynamic studies, the 1st and 4th pseudo components have $E_0$ of 189.6 and 180.6 kJ/mol and $\Delta G°$ of 191.7 and 169.3 kJ/mol, representing lignin decomposition. The 2nd pseudo component represents cellulose with an $E_0$ of 176.1 kJ/mol and $\Delta G°$ of 153.9 kJ/mol. The 5th pseudo component represents hemicellulose with an $E_0$ of 152.2 kJ/mol and $\Delta G°$ of 142.1 kJ/mol. The 3rd pseudo component represents the bound moisture or light volatile with an $E_0$ of 145.6 kJ/mol and $\Delta G°$ of 125.6 kJ/mol. The combination of multi-DAEM and DTA indicates that the thermal decomposition reactions in the 2nd, 3rd, and 5th pseudo components are endothermic, the 1st pseudo component is exothermic, and the 4th pseudo component is endothermic or possibly exothermic.

## 5. ACKNOWLEDGMENT

The author is grateful for the research grant provided by "The Directorate of Research, Technology, and Community Service from the Ministry of Education, Culture, Research, and Technology" as part of the National Competitive Basic Research (PDKN): plan for the Fiscal Year 2022, Number 001/PB.PDKN /BRIn.LPPM/VI/2022.

## 6. AUTHORS' NOTE

The authors declare that there is no conflict of interest regarding the publication of this article. The authors confirmed that the paper was free of plagiarism.

## 7. REFERENCES

Aamer, M., Ye, G., Luo, H., Liu, C., Malik, S., Afzal, I., Xu, J., and Sajjad, M. (2017). Bioresource technology pyrolysis and kinetic analyses of camel grass (Cymbopogon schoenanthus) for bioenergy. *Bioresource Technology*, *228*, 18–24.

Aboyade, A. O., Hugo, T. J., Carrier, M., Meyer, E. L., Stahl, R., Knoetze, J. H., and Görgens, J. F. (2011). Non-isothermal kinetic analysis of the devolatilization of corn cobs and sugar cane bagasse in an inert atmosphere. *Thermochimica Acta*, *517*(1–2), 81–89.

Bonilla, J., Salazar, R. P., and Mayorga, M. (2019). Kinetic triplet of Colombian sawmill wastes using thermogravimetric analysis. *Heliyon*, *5*(10), e02723.

Burnham, A. K., and Braun, R. L. (1999). Global kinetic analysis of complex materials. *Energy and Fuels*, *13*(1), 1-22.

Burra, K. G., and Gupta, A. K. (2018). Kinetics of synergistic e ff ects in co-pyrolysis of biomass with plastic wastes. *Applied Energy*, *220*, 408–418.

Cai, J., and Liu, R. (2007). Weibull mixture model for modeling nonisothermal kinetics of thermally stimulated solid-state reactions: Application to simulated and real kinetic conversion data. *The Journal of Physical Chemistry. B*, *111*, 10681–10686.

Cai, J., Wu, W., and Liu, R. (2014). An overview of distributed activation energy model and its application in the pyrolysis of lignocellulosic biomass. *Renewable and Sustainable Energy*

*Reviews*, *36*, 236–246.

Cai, J., Yao, F., Yi, W., and He, F. (2006). New temperature integral approximation for nonisothermal kinetics. *AIChE Journal*, *52*(4), 1554–1557.

Dhaundiyal, A., and Singh, S. B. (2016). Distributed activation energy modelling for pyrolysis of forest waste using gaussian distribution. *Proceedings of The Latvian Academy of Sciences Section B*, *70*(2), 64–70.

Feng, Y., Qiu, K., Zhang, Z., Li, C., Rahman, M., and Cai, J. (2022). Distributed activation energy model for lignocellulosic biomass torrefaction kinetics with combined heating program. *Energy*, *239*, 122228.

Guedes, R. E., Luna, A. S., and Torres, A. R. (2018). Operating parameters for bio-oil production in biomass pyrolysis: A review. *Journal of Analytical and Applied Pyrolysis*, *129*, 134–149.

Güneş, M., and Güneş, S. (1999). The influences of various parameters on the numerical solution of nonisothermal DAEM equation. *Thermochimica Acta*, *336*(1), 93–96.

Hameed, S., Sharma, A., Pareek, V., Wu, H., and Yu, Y. (2019). A review on biomass pyrolysis models: Kinetic, network and mechanistic models. *Biomass and Bioenergy*, *123*, 104–122.

Jamilatun, S., Budhijanto, Rochmadi, Yuliestyan, A., and Budiman, A. (2019). Valuable chemicals derived from pyrolysis liquid products of spirulina platensis residue. *Indonesian Journal of Chemistry*, *19*(3), 703–711.

Jamilatun, S., Pitoyo, J., Amelia, S., Ma, A., Hakika, D. C., and Mufandi, I. (2022). Experimental study on the characterization of pyrolysis products from bagasse (Saccharum Officinarum L .) : Bio-oil , biochar , and gas products. *Indonesian Journal of Science and Technology, 7*, 565–582.

Jiang, G., Nowakowski, D. J., and Bridgwater, A. V. (2010). A systematic study of the kinetics of lignin pyrolysis. *Thermochimica Acta, 498*, 61–66.

Jr, M., and Grønli, M. (2003). The art, science, and technology of charcoal production. *Industrial and Engineering Chemistry Research*, *42*, 1619–1640.

Kaczor, Z., Buliński, Z., and Werle, S. (2020). Modelling approaches to waste biomass pyrolysis: A review. *Renewable Energy*, *159*, 427–443.

Khajehzadeh, M., Ehsani, N., Baharvandi, H. R., Abdollahi, A., Bahaaddini, M., and Tamadon, A. (2020). Thermodynamical evaluation, microstructural characterization and mechanical properties of B4C–TiB2 nanocomposite produced by in-situ reaction of Nano-TiO2. *Ceramics International*, *46*(17), 26970–26984.

Kim, Y., Kim, Y., and Kim, S. (2010). Investigation of thermodynamic parameters in the thermal decomposition of plastic waste-waste lube oil compounds. *Environmental Science and Technology*, *44*, 5313–5317.

Kristanto, J., Mufti, M., and Purwono, S. (2021). Heliyon Multi-distribution activation energy model on slow pyrolysis of cellulose and lignin in TGA / DSC. *Heliyon*, *7*, e07669.

Kuo-Chao, L., Keng-Tung, W., Chien-Song, C., and Wei-The, T. (2009). A new study on combustion behavior of pine sawdust characterized by the weibull distribution. *Chinese*

DOI: https://doi.org/10.17509/ijost.v8i3.60175
p- ISSN 2528-1410 e- ISSN 2527-8045

*Journal of Chemical Engineering*, *17*(5), 860–868.

Lin, Y., Tian, Y., Xia, Y., Fang, S., Liao, Y., and Yu, Z. (2019). Bioresource technology general distributed activation energy model ( G-DAEM ) on co-pyrolysis kinetics of bagasse and sewage sludge. *Bioresource Technology*, *273*, 545–555.

Lin, Y.-C., Cho, J., Tompsett, G. A., Westmoreland, P. R., and Huber, G. W. (2009). Kinetics and mechanism of cellulose pyrolysis. *The Journal of Physical Chemistry C*, *113*(46), 20097–20107.

Mcguinness, M. J., Sciences, C., and Zealand, N. (1999). Asymptotic approximations to the distributed activation energy model. *Applied Mathematics Letters, 12*(1999),27-34.

Ordonez-Loza, J., Chejne, F., Jameel, A. G. A., Telalovic, S., Arrieta, A. A., and Sarathy, S. M. (2021). An investigation into the pyrolysis and oxidation of bio-oil from sugarcane bagasse: Kinetics and evolved gases using TGA-FTIR. *Journal of Environmental Chemical Engineering*, *9*(5), 106144.

Órfão, J. J. M. (2007). Review and evaluation of the approximations to the temperature integral. *AIChE Journal*, *53*, 2905–2915.

Pitoyo, J., Eka, T., and Jamilatun, S. (2022). Bio-oil from oil palm shell pyrolysis as renewable energy : A review. *Chemica, 9*(2), 67–79.

Pradana, Y. S., Daniyanto, Hartono, M., Prasakti, L., and Budiman, A. (2019). Effect of calcium and magnesium catalyst on pyrolysis kinetic of Indonesian sugarcane bagasse for biofuel production. *Energy Procedia*, *158*, 431–439.

Quan, C., Gao, N., and Song, Q. (2016). Journal of analytical and applied pyrolysis pyrolysis of biomass components in a TGA and a fixed-bed reactor : Thermochemical behaviors , kinetics , and product characterization. *Journal of Analytical and Applied Pyrolysis*, *121*, 84–92.

Quan, C., Li, A., and Gao, N. (2009). Thermogravimetric analysis and kinetic study on large particles of printed circuit board wastes. *Waste Management*, *29*(8), 2353–2360.

Sciacovelli, A., and Verda, V. (2012). Sensitivity analysis applied to the multi-objective optimization of a MCFC hybrid plant. *Energy Conversion and Management*, *60*, 180–187.

Sonobe, T., and Worasuwannarak, N. (2008). Kinetic analyses of biomass pyrolysis using the distributed activation energy model. *Fuel*, *87*, 414–421.

Sukarni, S. (2020). Thermogravimetric analysis of the combustion of marine microalgae Spirulina platensis and its blend with synthetic waste. *Heliyon*, *6*(9), e04902.

Terry, L. M., Li, C., Chew, J. J., Aqsha, A., How, B. S., Loy, A. C. M., Chin, B. L. F., Khaerudini, D. S., Hameed, N., Guan, G., and Sunarso, J. (2021). Bio-oil production from pyrolysis of oil palm biomass and the upgrading technologies: A review. *Carbon Resources Conversion*, *4*, 239–250.

Tran, K., Bui, H., and Chen, W. (2016). Distributed activation energy modelling for thermal decomposition of microalgae residues. *Chemical Engineering Transactions, 50*, 175–180.

Várhegyi, G., Bobály, B., Jakab, E., and Chen, H. (2011). Thermogravimetric study of biomass pyrolysis kinetics. A distributed activation energy model with prediction tests. *Energy*

DOI: https://doi.org/10.17509/ijost.v8i3.60175
p- ISSN 2528-1410 e- ISSN 2527-8045

*and Fuels*, *25*(1), 24–32.

Viju, D., Gautam, R., and Vinu, R. (2018). Application of the distributed activation energy model to the kinetic study of pyrolysis of Nannochloropsis oculata. *Algal Research*, *35*, 168–177.

Vyazovkin, S., Burnham, A. K., Criado, J. M., Pérez-Maqueda, L. A., Popescu, C., and Sbirrazzuoli, N. (2011). ICTAC kinetics committee recommendations for performing kinetic computations on thermal analysis data. *Thermochimica Acta*, *520*(1–2), 1–19.

Wang, S., Dai, G., Yang, H., and Luo, Z. (2017). Lignocellulosic biomass pyrolysis mechanism: A state-of-the-art review. *Progress in Energy and Combustion Science*, *62*, 33–86.

Wang, S., Ru, B., Lin, H., Sun, W., and Luo, Z. (2015). Pyrolysis behaviors of four lignin polymers isolated from the same pine wood. *Bioresource Technology*, *182*, 120–127.

Xu, Y., and Chen, B. (2013). Investigation of thermodynamic parameters in the pyrolysis conversion of biomass and manure to biochars using thermogravimetric analysis. *Bioresource Technology, 146*, 485–493.

Yang, H., Yan, R., Chen, H., Lee, D. H., and Zheng, C. (2007). Characteristics of hemicellulose, cellulose and lignin pyrolysis. *Fuel*, *86*(12–13), 1781–1788.

Zhang, J., Chen, T., Wu, J., and Wu, J. (2014). Multi-Gaussian-DAEM-reaction model for thermal decompositions of cellulose , hemicellulose and lignin : Comparison of $N_2$ and $CO_2$ atmosphere. *Bioresource Technology*, *166*, 87–95.

Zhang, Z., Shen, P., and Jiang, Q.-C. (2008). Differential thermal analysis (DTA) on the reaction mechanism in Fe–Ti–B4C system. *Journal of Alloys and Compounds*, *463*, 498–502.

Zhao, J. P., Tang, G. F., Wang, Y. C., and Han, Y. (2020). Explosive property and combustion kinetics of grain dust with different particle sizes. *Heliyon*, *6*(3), e03457.

DOI: https://doi.org/10.17509/ijost.v8i3.60175
p- ISSN 2528-1410 e- ISSN 2527-8045